Volume 1 | Number 1 | Jan 2013 | Pages 1–100

This is an *Accepted Manuscript*, which has been through the Royal Society of Chemistry peer review process and has been accepted for publication.

Accepted Manuscripts are published online shortly after acceptance, before technical editing, formatting and proof reading. Using this free service, authors can make their results available to the community, in citable form, before we publish the edited article. We will replace this *Accepted Manuscript* with the edited and formatted *Advance Article* as soon as it is available.

You can find more information about *Accepted Manuscripts* in the **Information for Authors**.

Please note that technical editing may introduce minor changes to the text and/or graphics, which may alter content. The journal's standard **Terms & Conditions** and the **Ethical guidelines** still apply. In no event shall the Royal Society of Chemistry be held responsible for any errors or omissions in this *Accepted Manuscript* or any consequences arising from the use of any information it contains.

Structural dependency of collagen fibers on ion types revealed by *in situ* second harmonic generation (SHG) imaging method

Xuye Lang and Julia G. Lyubovitsky

Ionic species in aqueous solutions alter protein solubility and aggregation behavior through a variety of complex interactions. Employing second harmonic generation (SHG) imaging in a backscattering configuration *in situ* we discovered that added phosphate modulates the aggregated collagen fibers' lengths within 3D hydrogels. For example, the about 1 μm in length collagen fibers formed in 30 mM phosphate-only buffer, 37 °C, 2 g/l collagen solid content extended to about 45 μm and increased in width in high (>/=60 mM) phosphate. Adding sodium sulfate in a 30 mM phosphate buffer to polymerize collagen into a hydrogel at 37 °C had similar effects. On the other hand, adding sodium chloride did not lengthen collagen fibers. The fiber lengths and widths decreased in very high concentrations of all salts. To establish the timescales of the involved polymerization processes, we used traditional turbidity measurements of gelation. Based on the solubility experiments we concluded that over 85% of collagen had precipitated under all experimental conditions. The non-invasive *in situ* SHG imaging in this study is valuable because it reduces the possibility of artifacts associated with changes to the fragile collagen hydrogels taking place in the conventional electron and optical imaging experiments.

Introduction

The exact mechanism of how salt ions and other charged species interact with proteins is not fully understood. These interactions, however, are known to modulate proteins' solubility and aggregation processes. There are many works to date that focused on the effects of ions on the water environment and described how it may affect protein stability in solutions and formation of nanostructures. Few studies explored the impact of the interactions on the fiber structures self-assembled at the microscopic scale. *In situ* non-invasive methods are needed to characterize the structures formed to understand the contributions of ions to the formation of the higher order assemblies that form microstructures within the biologically derived protein 3D scaffolds.

Collagen protein is a major component of the **extracellular** matrix (ECM) within the mammalian connective tissues. It accounts for approximately 20-30% of all protein in a human body.[1] Due to collagen ability to form fibers that contribute to stability within the polymeric networks, it remains a popular biomaterial choice for tissue engineering[2] and preparation of 3D scaffolds. Collagen protein undergoes a complex hierarchical organization at multiple length scales that range from triple-stranded helical collagen molecules to nano- (fibrils), micro- (fibers and fiber bundles) and macro- (gel) scales. Second harmonic generation (SHG) contrast serves as a valuable label-free spectroscopic probe that can be used to directly detect aggregated collagen structures (fibers) within scaffolds non-invasively and *in situ*. The SHG contrast results from an interaction between fibrillar collagen and near-infrared (NIR) pulsed, femtosecond laser light of scanning non-liner microscopy.[3] SHG is produced when photons interacting with fibrillar collagen are combined to form new photons with exactly twice the energy. The interaction between laser pulses and collagen's noncentrosymmetric, triple helix structure in addition to collagen packing within the materials leads to scattering from the tertiary (fibrils)[4] and quaternary (fibers)[5] level of collagen organization thus producing SHG[6] contrast. **Because NIR wavelengths are utilized,[7] it is possible to generate and image this contrast deep inside opaque 3D samples such as collagen hydrogels.** A significant advantage of SHG contrast is no bleaching and it had been employed to successfully image structural proteins with high resolution and contrast in biomedical assessment of tissue structure.[8]

We have examined with SHG contrast the contributions of different ions to collagen aggregation that forms microscopic fiber structures within three-dimensional (3D) hydrogels. To our knowledge, these studies represent first attempts to systematically study directly, non-invasively and *in situ* the effect of various ions on collagen fibers and hydrogel microstructure assembled with different salts. To gain insights into the structural changes associated with adding salts to proteins, we carried out such studies throughout a wide range of salt concentrations. We further combined our optical imaging experiments with traditional turbidity measurements of gelation to establish the timescales of the involved processes and solubility to assess the amount of collagen remaining in solution after completion of fibrogenesis.

Materials and Methods

Collagen Hydrogel Preparation

High concentration rat-tail type I collagen stock was obtained from BD Biosciences (354249), used as received and stored in 4 °C. **The polymerization process of collagen was started by mixing 2× fibrogenesis initiation buffer with 0.02 N acetic acid, collagen stock**

and adjusting the final pH of samples with 1 M NaOH to the pH = 7.4. The mixing process was done gently on ice. The samples were then incubated under experimental temperature (room temperature (RT), 27 °C or 37 °C).

We used Henderson-Hasselbalch equation (pH = pKa + log([base]/[acid])) to calculate the concentrations of mono- and dibasic phosphate for the pH = 7.4. At pH 7.4, the $[HPO_4]^{2-}$ ion is in 2 to almost 4 fold excess compared to $[H_2PO_4]^-$ ion. After the pH adjustment, all the buffers were filtered with 0.22 μm, 33 mm syringe filter (Millipore, Millex-GV, SLGV033RS).

For NaCl and Na$_2$SO$_4$ assisted collagen hydrogel assembly the salts were dissolved in 60 mM phosphate buffer (2× fibrillogenesis initiation buffer). The 2× fibrillogenesis initiation buffers were prepared by mixing buffer A and buffer B in the appropriated ratios. The composition of buffer A was 36 mM K$_2$HPO$_4$, 23 mM KH$_2$PO$_4$ and 1.8 M NaCl or 0.9 M Na$_2$SO$_4$. Buffer B contained only K$_2$HPO$_4$ and KH$_2$PO$_4$ at the same concentration as buffer A and was used to dilute the concentration of salt of buffer A to the appropriate 2× concentration values as needed.

The composition of the ionic species in the final mix was the following: 1) phosphate assembled collagen hydrogels - only phosphate buffer giving 5, 10, 20, 30, 40, 50, 60, 80, 100, 120, 140, 160, 180, 200, 300 and 500 mM concentrations; 2) NaCl assisted collagen hydrogel assembly - the final concentrations of NaCl employed to polymerize collagen hydrogels were 0, 150, 300, 600, 900 mM; 3) Na$_2$SO$_4$ assisted collagen hydrogel assembly - the final concentrations of Na$_2$SO$_4$ employed to polymerize collagen hydrogels were 0, 5, 10, 20, 50, 75, 100, 150, 300 mM. The measurement experiments on hydrogels prepared under these different conditions were repeated at least three times and/or on different days to verify reproducibility.

Solubility Measurements

For the solubility measurements, fibrillogenesis was carried out for 24 hours at the specified polymerization conditions and 2 g/l collagen solid content. Upon completion of fibrillogenesis, the samples were centrifuged at 12000 g for 5 minutes to separate precipitated collagen from soluble collagen molecules in the supernatant. We recorded the volume of the supernatant and measured the absorbance values at 218 nm. The absorbance values were converted to concentrations through dividing absorbance by an extinction coefficient value[9] of 9.43 mL•mg^{-1}•cm^{-1} and 1 cm pathlength of the cuvette. **The average values and standard deviations from the mean were calculated with Microsoft Excel.**

Turbidity Assays

The kinetics of collagen self-polymerization process was followed by detecting changes in turbidity at 450 nm. The samples were prepared as described in collagen hydrogel preparation section. After preparation, the samples were transferred into pre-chilled on ice cuvettes (NSG Precision Cells Inc., 9PS). We used temperature controlled UV-Vis-NIR spectrophotometer (Varian 500 Scan) to measure turbidity at the specified experimental temperature**s** (room temperature (RT), 27 °C or 37 °C). The turbidity was measured every 30 seconds until optical density (OD) value was stable for at least 20 minutes. From the kinetics curves, we determined delay times (Time$_{lag}$) which were the times needed to start the polymerization process, total times (Time$_{total}$), which were the times needed to complete the polymerization process, half times (Time$_{1/2}$), which were the times needed to get the half of maximum optical density (OD) values,

and maximum OD values. **The average values and standard deviations from the mean were calculated with Microsoft Excel.**

Second harmonic generation (SHG) imaging experiments

The samples were prepared according to the procedure described in collagen hydrogel preparation section. A silicon gasket was manually secured to the glass slide to prepare a chamber. The diameter of the chamber was 17 mm and the depth of the chamber was 2.2 mm. We placed the silicon chamber on ice. The liquid sample was introduced into the chamber and cover-slipped with NO.1 thickness coverglass. We incubated the sample under experimental temperature (room temperature (RT), 27 °C or 37 °C).

The upright multiphoton laser scanning microscope used to image collagen hydrogels in this work was the Thorlabs Multiphoton Microscope. It is based on an upright Nikon microscope equipped with a standard **illumination** system for the transmitted light. It was equipped with a femtosecond titanium:sapphire laser excitation source that provided femtosecond pulses at a repetition rate of about 80 MHz, with the center frequency tunable from 690 to 1040 nm. The long working distance immersion objectives (Zeiss, 63x water, N.A. 1.0; Zeiss, 10x water, N.A. 0.3; Olympus, 20x water, NA 1.0) were used to acquire images. The laser excitation used was linearly polarized at 810 nm. The two-photon signals from the samples were epi-collected and discriminated by the short pass 650 nm dichroic beamsplitter. Further spectral filtering with a dichroic (480 nm) and a 405±5 nm bandpass filter was used to separate the SHG signal. Each image presented is 2048 × 2048 pixels corresponding to 255 μm × 255 μm field of view for 63× images and about 1 mm × 1 mm for 10× images. **We generally collected about forty 2D images with a step size of 10 μm through the depth of 3D collagen hydrogels. Twenty to fifty representative fibers and pores were commonly selected from the collected images and measured using Image J (free open source Java image processing software developed at the National institutes of Health (http://rsb.info.nih.gov/ij/). The average values and standard deviations from the mean were then calculated with Microsoft Excel.** To obtain the second harmonic generation (SHG) signal averaged intensities as a function of penetration depth we used eight-chambered cover glass (MP Biomedicals, 09LX155411A) to prepare the samples **and** Olympus, 20× water, NA 1.0 objective **to image them. In these experiments the imaging parameters were kept the same. The laser power before the entrance into the microscope was 250 mW as measured with 818P Series Power Detector and 842-PE Optical Power/Energy Meter (Newport).** The home written Matlab code was used to evaluate SHG signal averaged intensities by calculating the average pixel values in the acquired images.

Results

To understand how salts influence polymerization of collagen into the aggregated 'fiber-like' structures as well as formation of hydrogels, we changed concentrations and kinds of salts in the polymerization mix.

37 °C phosphate assembled collagen hydrogels.

Polymerization and Kinetics. As the phosphate-buffer-induced-assembly proceeds from an optically transparent collagen solution into a scattering, semitranslucent hydrogel, there is an increase in the optical density (OD), which we detect at the wavelength of 450 nm. At this

wavelength, there is no measurable absorption from collagen and an increase in the OD values indicates formation of structures within hydrogels that scatter 450 nm light. At pH 7.4, 5 mM through 20 mM phosphate concentrations, instead of inducing hydrogel formation, precipitate collagen protein into small particles. These particles are detectable by eye. Because precipitated particles are randomly moving in and out of the excitation beam we could not detect an increase in turbidity in these samples.

Figure 1 and Table 1 summarize the effect of 30 mM – 200 mM phosphate on the polymerization of collagen into hydrogels. As seen in Figure 1, in agreement with somewhat similar prior experiments carried out on dilute solutions,[10, 11] increasing phosphate concentration (from 30 mM up to about 140 mM in our experiment) slows down collagen polymerization. However, there is no significant change in how long it takes to assemble collagen into hydrogels when phosphate is added at concentrations of 100 mM to 140 mM. Upon increasing the phosphate concentration beyond about 140 mM, polymerization of collagen speeds up and becomes noticeably faster when the concentration of phosphate reaches 200 mM. Based on the solubility measurements,[9, 12, 13] (Supplementary Figure S1) over 85% of collagen precipitates under all phosphate concentrations used in this work.

Second Harmonic Generation (SHG) Imaging. The second harmonic generation images show that the microstructure formed within collagen hydrogels depends strongly on the concentrations of phosphate present (Figure 2 and Supplementary Figure S2). For example, when concentration of phosphate is 30 mM, the fibers formed are very small (about 1 μm, Figure 2). When concentration of phosphate reaches 60 mM, few fibers extend in length (up to 15 μm, Figure 2). Upon further increasing the concentration of phosphate in a buffer solution, we observe a progressive shift in the fiber length and width towards larger values. For example in 160 mM phosphate, the fiber length and width are about 40 μm and 18 μm respectively (Figure 2). Upon further increasing the phosphate concentration we observe reduction in fiber widths and lengths. For example in 200 mM phosphate, the fiber length and width are about 17 μm and 1 μm respectively.

Sodium chloride assisted collagen hydrogel assembly.

Polymerization and kinetics. Figure 3 summarizes the contribution of 0 – 0.9 M sodium chloride to the polymerization of collagen into hydrogels. **Overall, the self-assembly rate does not appear to be affected by NaCl concentration and remains relatively constant for all conditions.** As seen in Figure 3A, when temperature is **37 °C**, 4 g/L collagen hydrogels' self-assembly rate (K, in units of min^{-1}) is somewhat faster compared to that observed for 2 g/L collagen hydrogels for most concentrations of sodium chloride. At the same time, for 4 g/L collagen samples' final OD values (Figure 3B) are also higher than for 2 g/L collagen hydrogels. The total time (Time $_{total}$ – Figure 3C) for 4 g/L samples' polymerizations are shorter compared to 2 g/L samples. Polymerization kinetics of 27 °C and room temperature (RT) assembled samples show trends similar to 37 °C assembly condition. When NaCl concentration is set at the physiological value of 0.15 M, we obtain the maximum OD value for every combination of temperature and collagen concentration. **Based on the solubility measurements, the amount of precipitated collagen is nearly 90% at 37 °C and is essentially the same at different sodium chloride concentrations.**

Second Harmonic Generation (SHG) Imaging. When incubation temperature is RT, for sodium chloride concentration of 0.9 M, collagen fibers formed are very small within both 2 g/l (Figure 4, top row) and 4 g/l (Supplementary Information Figure S3) hydrogels. When sodium chloride concentration is 0 M, collagen fibers formed are larger compared to when sodium chloride concentration is 0.9 M. However, for both, 2 g/l and 4 g/l collagen hydrogels, fibers formed with 0 M sodium chloride concentration are smaller compared to fibers induced with 0.3 to 0.6 M sodium chloride. For sodium chloride concentration of 0 M, the fibers formed are slightly longer in 2 g/l collagen hydrogels (up to about 45 μm) compared to 4 g/l collagen hydrogels (about 20 μm). When sodium chloride concentration is 0.3 M, the resulting effective pores within collagen hydrogels are clear (Figure 4) but for sodium chloride concentration of 0.6 M (not shown), the effective pores are filled with smaller fibers. For sodium chloride concentration of 0.3 M, the fiber lengths are about 50 μm within both 2 g/l and 4 g/l collagen hydrogels. On average, 0.3 M sodium chloride induced fibers within 2 g/l collagen hydrogels are slightly thinner compared to fibers within 4 g/l samples (about 3 μm versus 5 μm). An average diameter of the effective pores is about 60 μm within both 2 g/l and 4 g/l hydrogels prepared with 0.3 M sodium chloride.

The trend of how different sodium chloride concentrations affect the microstructure formation at 27 °C assembly temperature (Supplementary Figure S4) is similar to RT (Figure 4). When temperature is 27 °C, an average diameter of the effective pores formed at 0.3 M sodium chloride concentration (Supplementary Figure S4) is almost three times smaller compared to that observed at RT (about 22 μm versus about 60 μm). When temperature is 37°C (Figure 4, bottom row), the fibers formed are smaller than at RT and at 27°C. Nevertheless, the trend of how different sodium chloride concentrations affect the microstructure formation is similar to RT and 27 °C.

In summary, for all assembly temperatures, when sodium chloride concentrations are at the two extremes of 0 M and 0.9 M, the fibers formed are smaller compared to those formed at other sodium chloride concentrations under the same temperature and collagen solid content. For 0.9 M sodium chloride samples, the hydrogel's effective pore sizes are smaller than at other sodium chloride concentrations and some are too small to be reliably measured (Table 2). For samples polymerized at RT and 27 °C, for 0.3 M sodium chloride induced hydrogels, the effective pore structure is clear. On the contrary, there are many small fibers in the pore structure of 0.6 M sodium chloride samples at these incubation temperatures. In 0.3 M sodium chloride induced hydrogels, the fibers seem to be compacted better than in 0.6 M sodium chloride induced hydrogels. However, there are more connections between fibers in 0.6 M sodium chloride samples than in 0.3 M sodium chloride samples. When temperature is room temperature and sodium chloride concentration is 0.3 M, hydrogels have a good balance of fiber length, fiber width, effective pore structure and connections between fibers.

The relative scattering intensities and attenuation lengths (the depth into the hydrogel at which maximum SHG signal at the surface of the gel drops to $1/e$ of its value) of the prepared hydrogels are estimated from second harmonic generation (SHG) images. They are shown in Figure 5 (2 g/l hydrogels; A, B: 37 °C assembly; C, D: RT assembly). The maximum of the SHG intensities, which is related to the amount of scattering, shows similar trend to the optical density (OD) values obtained in turbidity measurements (Figure **3B**). As determined in this work, 37 °C 2 g/l hydrogels have 2 mm and greater attenuation lengths. These attenuation lengths do not appear to be significantly affected by difference in the amount of scattering between samples formed at different sodium chloride concentrations. RT 2 g/l hydrogels, 0 M sodium chloride samples are too heterogeneous to obtain practical decay data or the attenuation lengths. The

attenuation length shows both fast (about 100 μm) and slow (about 2 mm) decaying components for RT 2 g/l hydrogels induced with 0.3 M sodium chloride. They are about 500 μm and 1500 μm for RT 2 g/l hydrogels induced with 0.6 M sodium chloride and RT 2 g/l hydrogels induced with 0.9 M sodium chloride respectively. Multi-exponential decaying components recovered for the values of attenuation length in RT hydrogels indicate heterogeneity[14] in these samples.

Sodium sulfate assisted collagen hydrogel assembly.

Polymerization and kinetics. Upon incubation at 37 °C, the samples formed stable hydrogels at all Na_2SO_4 concentrations. The polymerization trends with sodium sulfate are similar to polymerization with phosphate (Table 1). For example, the total time to polymerize collagen into hydrogels first increases upon increasing salt concentration (from about 17 min to about 50 min in the sodium sulfate concentration range of 5 mM to 75 mM). The total time subsequently decreases to about 26 min when salt concentration is further increased to 150 mM.

Under the room temperature, collagen hydrogels assembled with different concentrations of Na_2SO_4 show three distinct regimes for the assembly. When Na_2SO_4 concentration is from 5 to about 50 mM, the measured delay times increase. When Na_2SO_4 concentration is from about 75 mM to 100 mM, the samples needed 7 to 10 days to polymerize. When Na_2SO_4 concentration is from 150 mM to 300 mM, the total time needed to polymerize hydrogels decreases along with increasing Na_2SO_4 content. The hydrogels formed under the room temperature are not homogenous by visual inspection.

Second Harmonic Generation (SHG) Imaging. For 2 g/l hydrogels polymerized at room temperature (RT), on average, fibers become longer and thinner if we change final Na_2SO_4 concentration from 5 mM (Figure 6, top row, left image and Table 3) to 20 mM (Table 3). However, 5 mM to 20 mM Na_2SO_4 induced hydrogles are not stable and samples imaged consist of fiber clusters dispersed in a somewhat liquid phase. When Na_2SO_4 concentration is from 75 mM to 100 mM, the samples take 7 − 10 days to partially polymerize. Therefore, we could not obtain images of the final products for this regime. When Na_2SO_4 concentration is from 150 to 300 mM, the total time needed to polymerize hydrogels decreases along with increasing Na_2SO_4 concentrations. The resulting fibers for 150 mM Na_2SO_4 are on the average longer and significantly thinner (Figure 6, top row, right image and Table 3) then in the first regime (5 mM to about 50 mM Na_2SO_4). The 4 g/l hydrogels polymerized at RT show similar trends (Table 3). In all three regimes, the RT polymerized hydrogels are not homogenous.

When polymerization temperature is 37 °C (Figure 6, bottom row), the hydrogels' microstructure is further altered. At this temperature, the microstructure of 2 g/l collagen hydrogels prepared with 5 mM Na_2SO_4 consists of some elongated fibers dispersed within material that does not produce strong second harmonic generation (SHG) signals. The somewhat smaller, however better defined SHG generating structures are observed within 4 g/l hydrogels (not shown) prepared under the same concentration of Na_2SO_4. A dense network of elongated fibers is seen in the SHG images of 2 g/l hydrogels prepared with 20 mM Na_2SO_4. On average, within 4 g/l hydrogels (not shown), fibers prepared at this Na_2SO_4 concentration appear slightly shorter and more densely packed. When Na_2SO_4 is 150 mM, similar to the phosphate-modulated polymerization, we observe substantially larger effective pores within both 2 g/l (Figure 6, bottom row, right image) and 4 g/l hydrogels (not shown) compared to lower concentration of sulfate.

Discussion

Mixing an initiation buffer solution which contains **dissolved** ions with stock collagen protein solution and adjusting pH of the mix to 7.4 initiates self-assembly of collagen within forming hydrogels. Upon completion of the collagen polymerization process within these colloidal systems, fiber is a salted out fraction or a floc consisting of collagen protein.

Ions' ability to salt out or salt in proteins in solutions is ordered into the Hofmeister series.[15] The series can be applied to understand interactions among ions, water and macromolecules such as proteins in bulk solutions as well as at the interface.[16] The classical anion series are arranged as $SO_4^{2-} > HPO_4^{2-} > CH_3COO^- > OH^- > F^- > Cl^- > Br^- \approx NO_3^- > I^- > ClO_4^- > SCN^-$. The strongly hydrated anions, which have stabilizing effect and decrease solubility of proteins (salt out), are to the left of Cl^-. The weakly hydrated anions to the right of Cl^- are protein denaturants, which increase protein solubility (salt in) upon interaction. The divalent anions HPO_4^{2-} and SO_4^{2-} employed in this study are early in the Hofmeister series. Compared to monovalent Cl^- anion, which is later in the series, they carry a greater capacity to decrease the solubility of collagen molecules and to promote aggregation.

In spite of many works of the past decade, the specific salting out effects of different ions with respect to the protein structure are poorly understood and lack systematic explanation.[16] However, there is consensus that a type and a concentration of added salts are the driving forces behind aggregation behavior.[16] The two processes potentially explaining this behavior that can take place simultaneously are: (i) the attenuation of electrostatic repulsion through the specific association of ions with proteins' charged groups and (ii) the ions altering the tension at the protein-aqueous interfaces. Association of anions with positively charged protein residues reduces the effective surface charges on the protein macromolecules. Larger (softer) anions are more efficient at screening the electrostatic repulsion between protein molecules and promoting salting-out behavior. Additionally, the surface tension of water increases along with an increase in the amount of salt[17] added thus stabilizing flocs[18] – collagen protein molecules and/or fibrils aggregated into the "fiber-like" structures observed in the second harmonic generation (SHG) images. Thus increased surface water tension and attenuated electrostatic repulsion due an increased amount of salt in the final polymerization mix can potentially lead to an increased size of the aggregated collagen flocs (fibers).

Under low phosphate concentrations (less than 20 mM), stable collagen hydrogels did not form and samples were essentially liquid. Along with inability to form stable gels, similar to previous studies, we observed an increase in collagen solubility in this range of phosphate concentrations. Kuznetsova et al.[19] referred to phosphate ions being strong fibrillogenesis inhibitors in the range of 10 to 25 mM and leading to an increase in collagen solubility. Subsequent studies by Mertz et al.[20] attribute this increase in solubility to the preferential interaction of the dibasic form of phosphate with collagen fibrils. The same study determined from infrared measurements that under physiological conditions there are one to two sulfate and dibasic phosphate binding sites per collagen molecule inside fibrils and none for the monovalent phosphate. The researchers proposed that bound divalent anions formed salt bridges between positively charged amino acid residues within the collagen fibrils. However, the study further suggested that this binding is insignificant to the formation, stability and structure of collagen fibrils and that the fibrils are stabilized by preferential exclusion of non-bound anions from interstitial water within fibrils. NaCl was proposed to affect binding of dibasic phosphate and partitioning of monobasic phosphate in collagen fibrils.

When we increased the phosphate concentration to about 30 mM – 60 mM, we formed stable hydrogels. Similarly to prior work on collagen assembly in diluted protein solutions (0.1 g/l),[11] we observed a decrease in collagen polymerization rate when phosphate concentration was increased beyond 30 mM. The fibers in 30 mM – 60 mM phosphate concentration range remained small. We believe that aggregation into the larger fiber structures is unfavorable in this phosphate concentration range due to only a modest disruption of the hydration shell of water around protein packed into the fiber structures. When phosphate concentration was high (80 – 160 mM), the phosphate in addition to maintaining the pH and binding to collagen molecules, must be significantly compressing the hydration shell within collagen fibers. The interactions of protein groups with salt can potentially make it easier for the fibrils to stick to each other to form a larger 'fiber' floc. This possibly explains why fibers are larger under this phosphate concentration compared to 30 – 60 mM phosphate–induced samples. Yet, increasing phosphate concentration further (200 or 300 mM) induced again smaller 'fiber-like' features within hydrogels. Very high phosphate concentrations (500 mM) resulted in the formation of fine precipitate along with slight increase in solubility. Proteins are often denatured by high concentrations of inorganic salts.[21] The ions formed due to dissolution of inorganic salts are possibly binding to ionic groups of proteins and disrupting interactions that stabilize collagen 'fiber-like' structures. These interactions lead to the formation of fine precipitate. Similar insight can be applied to the sodium sulfate and sodium chloride assisted collagen materials assembly at 37 °C. In those samples, there was enough phosphate to maintain the pH and to stabilize collagen fibers. Similarly, high concentration of 0.9 M NaCl appeared to encourage collagen solubility and led to the formation of smaller 'fiber' flocs.

In general in self-assembling systems, lowering or raising temperature affects formation of colloidal flocs in different and not obvious ways. This further raises a need to conduct measurements on such systems directly, non-invasively and *in situ*. The optical methods presented in this study are perfectly suited for such task. In a sodium-chloride-assisted collagen materials assembly at lower temperature (27 °C and/or room temperature) we observed formation of longer and thicker "fiber-like" structures compared to 37 °C assembled gels. Lowering temperature is potentially improving an exothermic adsorption step thus leading to the formation of larger "fiber-like" aggregates seen at 27 °C and room temperature. Interestingly, when a divalent anion such as sulfate is used, in the 5 mM – 20 mM concentration range of sulfate, large and long fibers are formed at room temperature. However, for these sulfate concentrations, a stable polymeric network within gels is not established perhaps due to insufficient overlap between the formed fibers. It is only more challenging to obtain a stable hydrogel in 75 mM to 100 mM sulfate since they did not seem to polymerize within even a few days. When sodium sulfate concentration was from 150 to 300 mM, the total time needed to polymerize hydrogels decreased along with increasing salt concentrations. The fibers were significantly thinner and somewhat longer then when sulfate was 5 mM – 20 mM. Further experiments are carried out to understand these complex phenomena resulting from combined effects of **polymerization** temperature,[5, 14] pH,[22, 23] **collagen solid content**[14] and ionic species on the self-assembly of collagen at the fiber structural level.

The studies presented in this work are timely. Recently, Li et al.[24] also studied collagen molecular interactions with a focus on fibrils formed in various salts dissolved directly in the collagen solutions adjusted to the appropriate pH with 0.1 M NaOH. Based on the low resolution **transmission electron microscopy (**TEM**)** images **the authors** concluded that at pH 7.4, low concentrations of salts that have monovalent ions lead to the formation of small filaments

without banding patterns. When the ionic strength was increased to 200 mM, the collagen fibrils were more ordered and some large fibrils with the banding patterns were observed. When salts with multivalent ions were used, collagen monomers aggregated to form ordered fibril bundles that showed **clearer** banding pattern**s**. Polarized light microscopy images of dispersed on glass slide**s** collagen fibrils formed in NaCl and KCl salts (100 mM, pH 7.4) and about 80 μm in diameter fibril bundles detected in Na_2SO_4 and Na_2HPO_4 samples (ionic strength 250 mM, pH 7.4) were **also** obtained.

In a somewhat related study, Jiang et al.[25] evaluated the effects of pH and electrolytes on the assembly of collagen into microribbons (about 3 nm anisotropic ribbon-like structures) deposited onto freshly cleaved mica supports. The deposition was controlled by employing hydrodynamic flow and the structures formed were examined with atomic force microscopy (AFM). The influence of $MgCl_2$, NaCl and KCl electrolytes on the assembly was studied at the neutral pH of 7.5. Interestingly, low NaCl concentration (50 mM) and high NaCl concentration (200 mM) resulted in single layer of collagen fibrils on the mica surface. However, when NaCl concentration was 100 mM, the protrusions of the first layer merged into incomplete second fibrillar layer.

Gobeaux et al.[26] also recently studied polymerization of collagen from concentrated solutions (40–300 mg/ml) at different pHs and ionic strengths. Two methods were used to adjust ionic strength. One method was to increase the concentration of phosphate buffer from 10 to 500 mM. Alternative method was to add NaCl in a 200 mM phosphate buffer. The gels formed in low ionic strength (24 mM) consisted of a dense network of 15–20 nm wide and 200–250 nm long nanofibrils observed in low resolution transmission electron microcopy (TEM) images. The fibrils increased in size and formed bundles as the ionic strength increased up to 261 mM along with an increase in gels' strength and opacity. Similarly, Harris et al.[27] concluded that at pH 7.0 and 8.0, in presence of 150 mM NaCl, the characteristic 67 nm D-banded collagen fibrils organized into fiber bundles predominated. At 529 mM and 1300 mM ionic strengths, Gobeaux et al.[26] study found that the polymerized collagen systems were biphasic. Specifically, at 529 mM ionic strength, large fibrillar bundles were surrounded by nanofibrils (about 40 nm in width and about 600 nm in length). On the other hand, at 1300 mM ionic strength the nanofibrils were surrounded by larger fibrils. The authors reported similar structures when monovalent salt was used to adjust the ionic strength.

Non-destructive *in situ* SHG imaging-based methods furnish new structural information regarding gross microscopic morphology of the synthesized collagen hydrogels. **In our studies, collagen hydrogels** were several millimeters in thickness. The structural information presented in this work is not attainable from **transmission electron microscopy (**TEM**) methods used by prior investigations**. TEM imaging is generally destructive to biological samples and requires transmission of the **electron** beams through ultra-thin specimens. Unlike prior studies,. Using SHG imaging, we assessed the parameters relevant to the structure of collagen fibers *in-situ* without disturbing materials. For example, unlike the study by Li et al.[24] we did not need to smear samples on the glass substrates to form thin sections in order to pass the transmitted light to form optical images.

To quantify relative differences in the hydrogels' microstructural parameters, we used a straight forward method of measuring the resulting fibers and effective pore sizes. While we reproducibly attain the measured numbers, the data analysis can greatly benefit from implementing automated methods. Some recent automatated approaches to analyze

the 2D SHG images include works of Bayan et al.[28] and Matteini et al.[29] which employed Fourier transform and entropy analysis methods to obtain information regarding orientation of collagen fibers in gels and cornea respectively. While these methods can work well for the thin and/or linear fibers, these approaches tend to be more global type of comparisons. It is not clear how to take into account the width of the fibers for larger/spreading fibers that we observed at the lower temperature. Texture analyses have also been employed to analyze the SHG images of the collagen structure within extracellular matrix of normal ovarian stroma and high grade ovarian serous cancer.[30] Another method recently developed and used to analyze collagen structure in 3D employs operators from mathematical morphology to obtain fiber orientations and radius distributions.[31]

The attenuation lengths parameters presented in this manuscript help to establish design criteria to construct hydrogels for applications in which imaging directly through such materials is anticipated. Our measurements indicate that 37 °C hydrogels we prepared are homogeneous and have great transparency using the imaging conditions we employ. When these gels were used topically on the mice skin, they did not impact imaging of the underlying either epidermal or deep dermal structures.

Endogenous fields and currents occur naturally due to presence of ions in the wounds in order to guide cell migration.[32, 33] It is conceivable therefore to envision the data and methods developed to be useful in examining the wound healing process where newly synthesized collagen aggregation process could be under ionic regulation. Manufacturing medical devices for bone tissue repair requires interactions of ionic regions of inorganic molecules of hydroxyapatite with collagen at the surfaces of fibrils/fibers[34-36] during its crystallization onto them and will potentially benefit from this research as well. The studies presented are also scientifically important and relevant to the field of tissue engineering as well, especially in the context of using ions as therapeutic agents.[37, 38]

Conclusion

The second harmonic generation (SHG) imaging *in situ* allowed us to determine that increasing concentrations of phosphate increase the lengths of 37 °C, pH 7.4 polymerized collagen fibers. When increasing concentrations of sodium sulfate are added to 30 mM phosphate buffer used to polymerize collagen into hydrogels, fiber lengths similarly increase. On the other hand, adding sodium chloride at physiological and higher concentrations does not significantly lengthen the fibers within 37 °C, pH 7.4 polymerized hydrogels. Lowering temperature leads to a multilateral response, which depends on the type of ion employed. The fiber lengths and widths decrease in very high concentrations of all salts at all temperatures. Traditional turbidity measurements provided timescales for the gelation processes examined and solubility data showed that 85% of collagen was precipitated under all experimental conditions. Ions are an important element to take into account when gelation of collagen and other biologically derived protein scaffolds takes place. The methods and knowledge presented in this work can be applied to understand these practically important and complex assembly processes.

Figure captions

Figure 1. The effect of different concentrations of phosphate on turbidity and kinetic parameters during collagen self-assembly into a 2 g/l hydrogel at pH 7.4, 37 °C. (A) Typical turbidity–time curves and corresponding standard deviations of the mean during collagen self-assembly. (B) The rate constants (K, in units of min^{-1}) of collagen self-assembly evaluated by fitting the slopes of turbidity curves like those shown in (A). (C) The observed final optical densities as a function of final phosphate concentration **and corresponding standard deviations from the mean**. (D) The times to the beginning ($Time_{lag}$), middle ($Time_{1/2}$) and completion ($Time_{total}$) of collagen self-assembly **and corresponding standard deviations from the mean**.

Figure 2. (Top row) Backscattered second harmonic generation (SHG) images from collagen hydrogels assembled at pH 7.4, 37 °C and different phosphate concentrations; (Bottom row) Quantification of collagen hydrogel parameters: fiber lengths, widths and effective pore sizes **and corresponding standard deviations from the mean.**

Figure 3. The effect of initial collagen concentrations, incubation temperatures and concentrations of sodium chloride on the kinetic parameters during collagen self-assembly into the fibers at pH 7.4, 30 mM phosphate. (A) The rate constants (K, in units of min^{-1}) of collagen self-assembly evaluated by fitting the slopes of turbidity curves. (B) The observed final optical densities as a function of final sodium chloride concentration **and corresponding standard deviations from the mean**. (C) The times ($Time_{total}$) to the completion of collagen self-assembly **and corresponding standard deviations from the mean**.

Figure 4. Backscattered second harmonic generation (SHG) images from 2 g/l collagen hydrogels assembled at pH 7.4, 30 mM phosphate and different sodium chloride concentrations as indicated. (Top row): room temperature (RT) assembly; (Bottom row): 37 °C assembly. The effective pore is indicated **with text** and the fiber is indicated with an arrow.

Figure 5. Backscattered second harmonic generation (SHG) signal averaged intensities plotted as a function of penetration depth (A), (C) and attenuation lengths (B), (D) in 2 g/l hydrogels assembled with 30 mM phosphate and different sodium chloride concentrations; (A) and (B) 37 °C assembly; (C) and (D) room temperature (RT) assembly. Lines are fits to the single exponential decays.

Figure 6. Backscattered second harmonic generation (SHG) images from 2 g/l collagen hydrogels assembled at pH 7.4, 30 mM phosphate and different sodium sulfate concentrations as indicated. (Top row): room temperature (RT) assembly. Red line indicates that fibers imaged correspond to different assembly regimes influenced by sodium sulfate concentration; (Bottom row): 37 °C assembly.

Table 1. Summary of the effect of 30 mM – 200 mM phosphate on the polymerization of collagen into a hydrogel at 37 °C, 2 g/l solid content, pH 7.4 **and corresponding standard deviations from the mean.**

Table 2. Summary of the collagen hydrogel microstructural parameters upon sodium chloride assisted assembly at pH 7.4, 30 mM phosphate, different temperatures and collagen solid content (2 g/l or 4 g/l) **and corresponding standard deviations from the mean.**

Table 3. Summary of the collagen hydrogel microstructural parameters upon sodium sulfate assisted assembly at pH 7.4, 30 mM phosphate, different temperatures and different collagen solid content (2 g/l or 4 g/l) **and corresponding standard deviations from the mean.**

Supporting Information: Supplementary Figure S1 (Supplementary Information Page S-2) shows the solubility of collagen in samples prepared under **37 °C** and different concentrations of phosphate. Supplementary Figure S2 (Supplementary Information Page S-3) shows additional backscattered second harmonic generation (SHG) images from collagen materials assembled at pH 7.4, 37 °C and 40 mM, 50 mM, 80 mM, 100 mM, 120 mM, 140 mM, 180 mM, 300 mM and 500 mM phosphate concentrations. Supplementary Figure S3 (Supplementary Information Page S-4) shows backscattered second harmonic generation (SHG) images from collagen materials assembled at pH 7.4, 4 g/l collagen solid content, room temperature as well as 37 °C and different sodium chloride concentrations. Supplementary Figure S4 (Supplementary Information Page S-4) shows backscattered second harmonic generation (SHG) images from collagen materials assembled at pH 7.4, 27 °C, different sodium chloride concentrations and quantification of the collagen hydrogel parameters.

References

1. R. D. Harkenss, *Biol. Rev.*, 1961, **36**, 399-455.
2. C. H. Lee, A. Singla and Y. Lee, *Int. J. Pharm.*, 2001, **221**, 1-22.
3. W. R. Zipfel, R. M. Williams and W. W. Webb, *Nature Biotech.*, 2002, **21**, 1367-1377.
4. R. M. Williams, W. R. Zipfel and W. W. Webb, *Biophys. J.*, **2005**, **88**, 1377-1386.
5. C. B. Raub, V. Suresh, T. B. Krasieva, J. G. Lyubovitsky, J. D. Mih, A. J. Putnam, B. J. Tromberg and S. C. George, *Biophys. J.*, 2007, **92**, 2212-2222.
6. S. Roth and I. Freund, *J. Chem. Phys.*, 1979, **70**, 1637-1643.
7. W. R. Zipfel, R. M. Williams, R. Christie, A. Y. Nikitin, B. T. Hyman and W. W. Webb, *Proc. Natl. Acad. Sci. U.S.A.* , 2003, **100**, 7075–7080.
8. F. Legare, C. Pfeffer and B. R. Olsen, *Biophys. J.*, 2007, **93**, 1312-1320.
9. G. C. Na, L. J. Butz, D. G. Bailey and R. J. Carroll, *Biochemistry* 1986, **25**, 958-966.
10. H. B. Bensusan and B. L. Hoyt, *J. Am. Chem. Soc.*, 1958, **58**, 719-724.
11. B. R. Williams, R. A. Gelman, D. C. Poppke and K. A. Piez, *J. Biol. Chem.*, 1978, **253**, 6578-6585.
12. J. Hirshburg, B. Choi, S. Nelson and A. T. Yeh, *J. Biomed. Opt. Letters*, 2006, **11**, 040501-040501.
13. J. Hirshburg, B. Choi, S. Nelson and A. T. Yeh, *Lasers in Surgery and Medicine* 2007, **39**, 140-144
14. Y. Hwang and J. G. Lyubovitsky, *Anal. Meth.*, 2011, **3**, 529-536.
15. F. Hofmeister, *Arch. Exp. Pathol. Pharmakol.*, 1888, **24**, 247−260.
16. P. L. Nostro and B. W. Ninham, *Chem. Rev.*, 2012, **112**, 2286-2322.
17. N. L. Jarvis and M. A. Scheiman, *J. Phys. Chem.*, 1968, **72**, 74-78.
18. P. C. Hiemenz *Principles of colloid and surface chemistry*, 2nd ed.; M. Dekker: New York, 1986.
19. N. Kuznetsova, S. L. Chi and S. Leikin, *Biochemistry* 1998, **37**, 11888-11895.
20. E. L. Mertz and S. Leikin, *Biochemistry*, 2004, **43**, 14901-14912.
21. I. Palmer and P. T. Wingfield, *Curr. Protoc. Protein Sci.*, 2004, **38**, 6.3.1-6.3.18.
22. C. B. Raub, J. Unruh, V. Suresh, T. Krasieva, T. Lindmo, E. Gratton, B. J. Tromberg and S. C. George, *Biophys. J.* , 2008, **94**, 2361-2373.
23. S. Bancelin, C. Aimé, T. Coradin and M. C. Schanne-Klein, *Biomed. Opt. Express*, 2012, **3**, 1446.
24. Y. Li and E. P. Douglas, *Colloids Surf., B* 2013, **112**, 42-50.
25. F. Z. Jiang, H. Hörber, J. Howard and D. J. Müller, *J. Struct. Biol.* , 2004, **148**, 268-278
26. F. Gobeaux, G. Mosser, A. Anglo, P. Panine, P. Davidson, M.-M. Giraud-Guille and E. Belamie, *J. Mol. Biol.*, 2008, **376**, 1509-1522.
27. J. R. Harris and A. Reiber, *Micron*, 2007, **38**, 513-521
28. C. Bayan, J. M. Levitt, E. Miller, D. Kaplan and I. Georgakoudi, *J. App. Phys.*, 2009, **105**, 102042.
29. P. Matteini, F. Ratto, F. Rossi, R. Cicchi, C. Stringari, D. Kapsokalyvas, F. S. Pavone and R. Pini, *Opt. Express* 2009, **17**, 4868-4878
30. B. L. Wen, M. A. Brewer, O. Nadiarnykh, J. Hocker, V. Singh, T. R. Mackie and P. J. Campagnola, *J. Biomed. Opt.*, 2014, **19**, 096007.
31. H. Altendorf, E. Decencière, D. Jeulin, P. De Sa Peixoto, A. Deniset-Besseau, E. Angelini, G. Mosser and M.-C. Schanne-Klein, *J. Microscopy* 2012, **247**, 161-175.
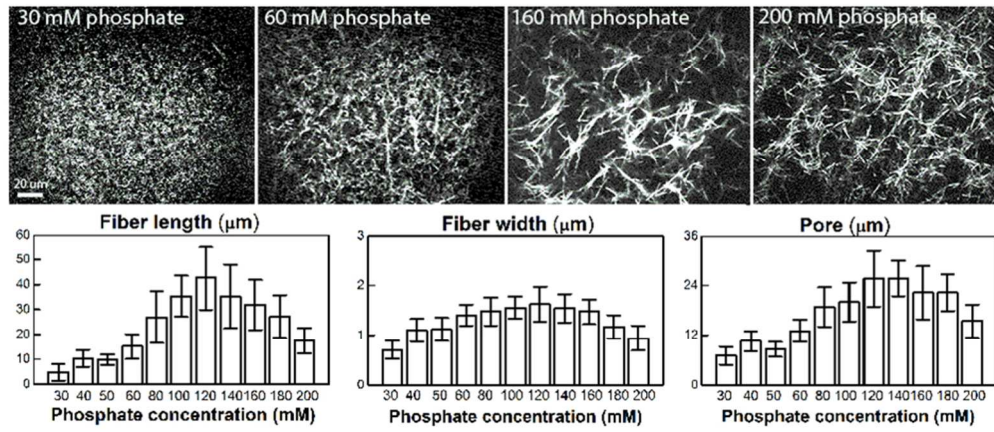32. B. Reid, B. Song, C. D. McCaig and M. Zhao, *Faseb. J.*, 2005, **19**, 379-386.

33.   A. C. Vieira, B. Reid, L. Cao, M. J. Mannis, I. R. Schwab and M. Zhao, *PLoS One*, 2011, **6**, e17411.

34.   S. Weinera and W. Traubb, *FEBS Letters*, 1986, **206**, 262–266.

35.   N. Roveri, G. Falini, M. C. Sidoti, A. Tampieri, E. Landi, M. Sandri and B. Parma, *Mater. Sci. Eng. C*, 2003, **23**, 441-444.

36.   D. A. Wahl and J. T. Czernuszka, *European Cells and Materials*, 2006, **11**, 43-56.

37.   D. S. Adams, *Tissue Eng. Part A.* , 2008 **14**, 1461-1468.

38.   V. Mouriño, J. P. Cattalini and A. R. Boccaccini, *J. of R. Soc. Interface*, 2012, **9**, 401-419.
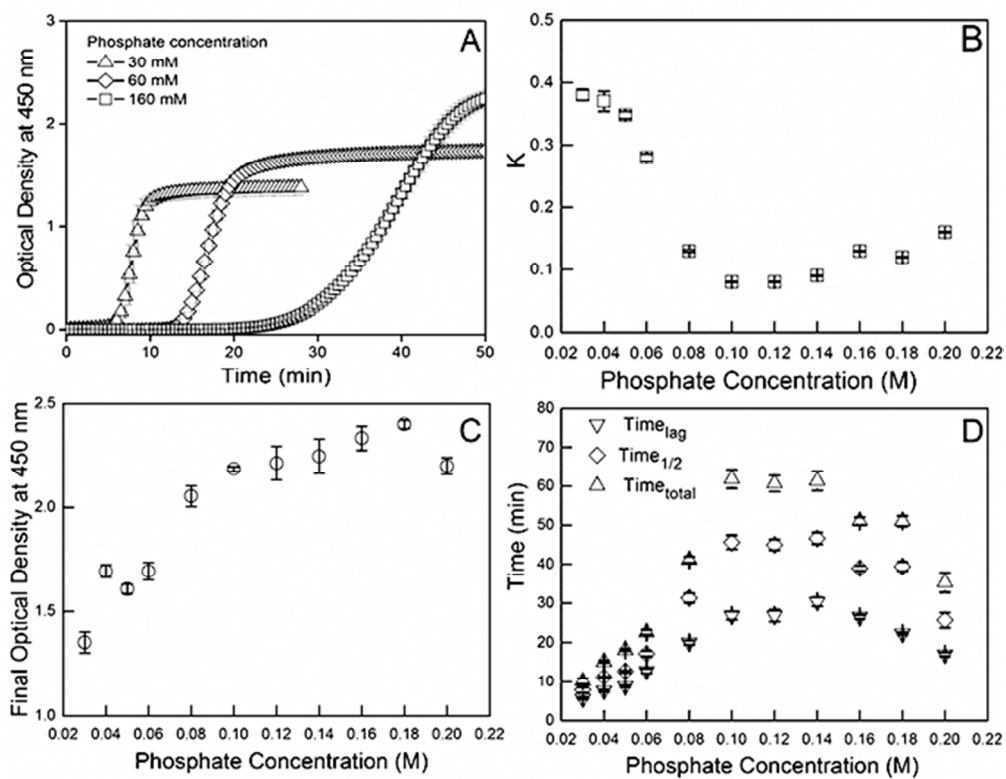
Figure 1.

239x197mm (72 x 72 DPI)

Figure 2

249x112mm (96 x 96 DPI)
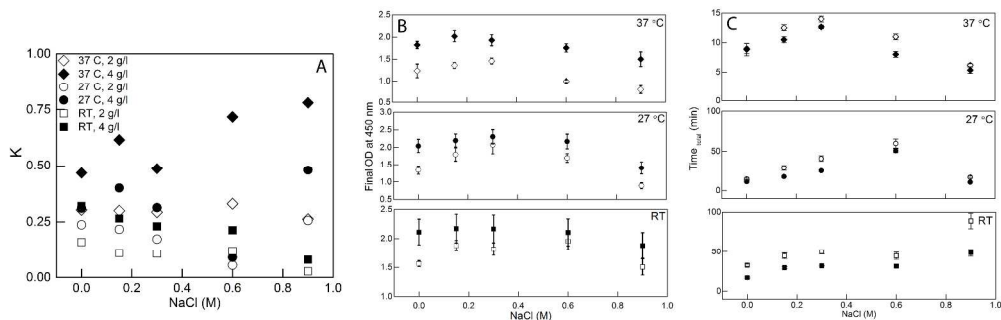
672x222mm (295 x 295 DPI)
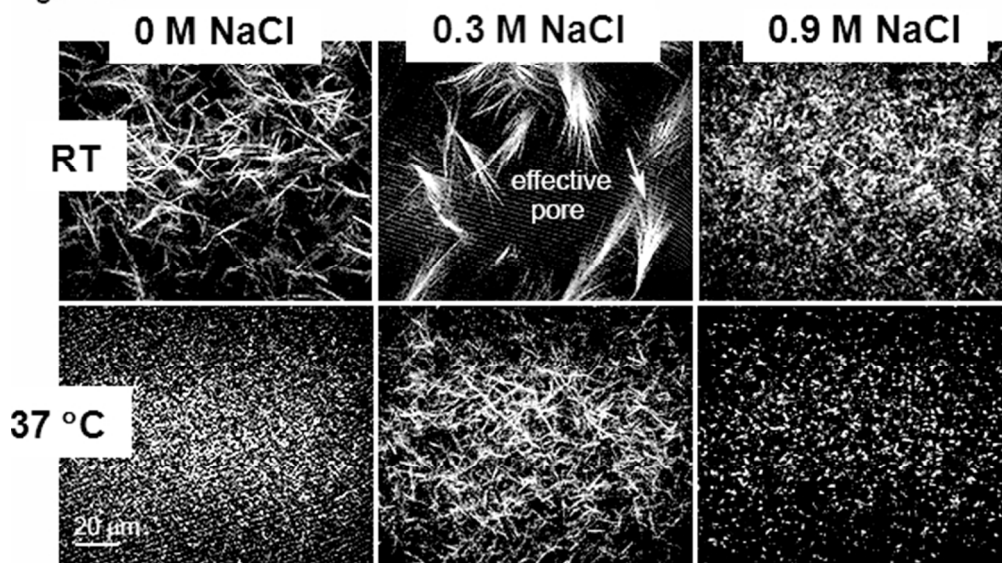
Figure 4

163x98mm (96 x 96 DPI)
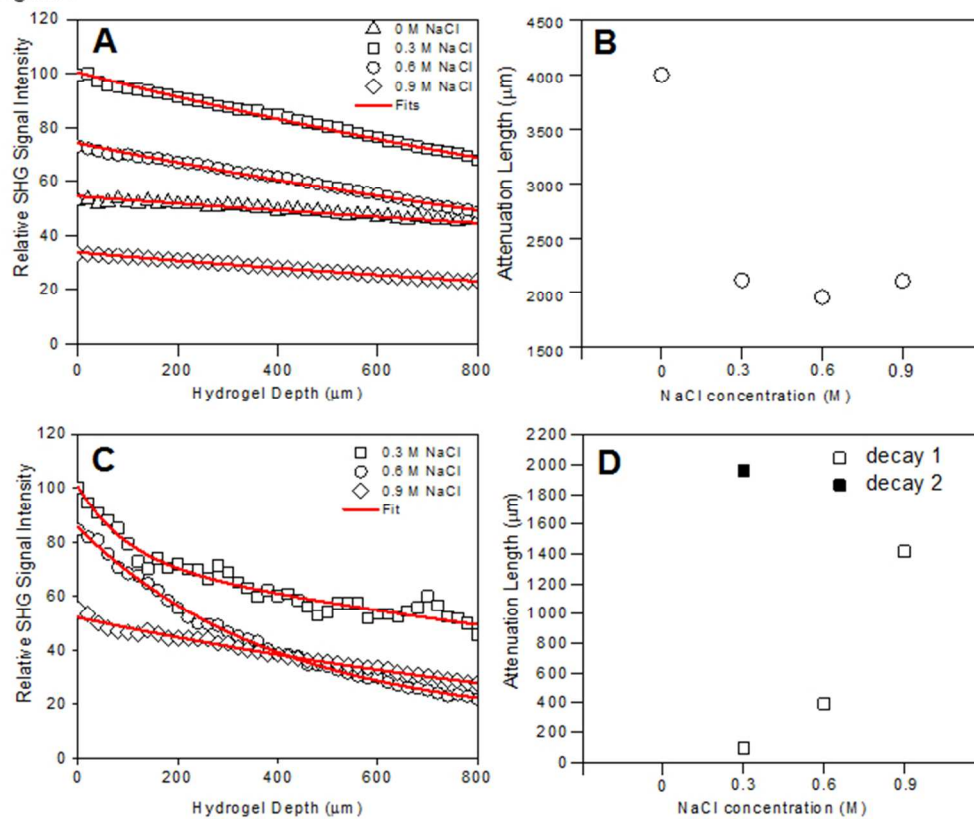
Figure 5

183x154mm (96 x 96 DPI)

Figure 6
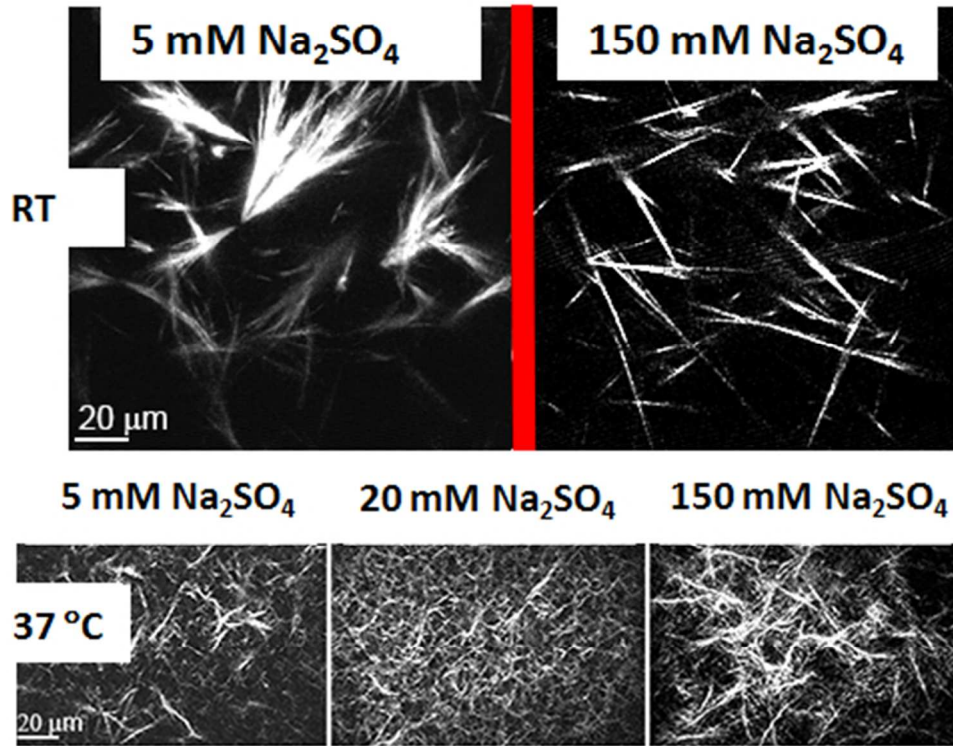
128x106mm (96 x 96 DPI)

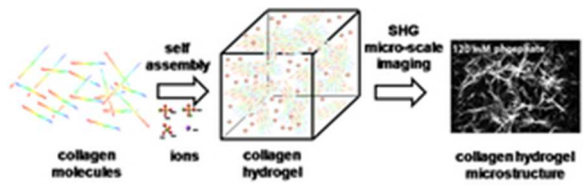| Phosphate Concentration (mM)	Delay Time (min)	Half Time (min)	Total Time (min)	OD Value (min)	Rate (min^{-1})
30	5.7 ± 0.29	7.87 ± 0.65	10.2 ± 0.76	1.4 ± 0.05	0.38 ± 0.016
40	7.7 ± 0.29	11.2 ± 0.27	15.2 ± 0.29	1.7 ± 0.03	0.37 ± 0.006
50	8.8 ± 0.29	12.7 ± 0.27	18.2 ± 0.29	1.6 ± 0.02	0.35 ± 0.006
60	12.8 ± 0.60	17.2 ± 0.72	22.7 ± 0.57	1.7 ± 0.04	0.28 ± 0.002
80	20.0 ± 0.50	31.3 ± 1.20	41.2 ± 0.76	2.1 ± 0.05	0.13 ± 0.001
100	26.8 ± 1.04	45.6 ± 1.77	61.8 ± 2.47	2.2 ± 0.01	0.08 ± 0.001
120	26.8 ± 1.53	44.9 ± 1.37	60.7 ± 2.08	2.2 ± 0.08	0.08 ± 0.001
140	30.3 ± 1.15	46.6 ± 1.51	61.3 ± 2.52	2.2 ± 0.08	0.09 ± 0.001
160	26.5 ± 0.50	38.9 ± 0.66	51.0 ± 1.00	2.3 ± 0.06	0.13 ± 0.001
180	22.3±0.29	39.4±1.15	51.0±1.32	2.4±0.02	0.12±0.001
200	17.0±0.50	25.7±1.91	35.3±2.51	2.2±0.04	0.16±0.001

1
2
3
4
5
6
7
8
9
10
11
12
13
14
15
16
17
18
19
20
21
22
23
24
25
26
27
28
29
30
31
32
33
34
35
36
37
38
39
40
41
42
43
44
45
46
47
48
49
50
51
52
53
54
55
56
57
58
59
60

Condition Temperature, Solid content	[NaCl]=0 M Fiber Length Fiber Width Pore Size (µm)	[NaCl]=0.3 M Fiber Length Fiber Width Pore Size (µm)	[NaCl]=0.6 M Fiber Length Fiber Width Pore Size (µm)	[NaCl]=0.9 M Fiber Length Fiber Width Pore Size (µm)
RT, 2 g/l	34.3±10.2 1.7±0.3 18.7±8.7	52.0±12.1 2.5±0.8 60±13	42.4±9.3 2.5±0.9 22.3±4.7	2.6±1.2 0.2±0.1 3.9±1.3
RT, 4 g/l	20.4±4.7 1.3±0.4 10.0±2.6	50.0±7.4 5.2±1.4 60±11.5	35.7±5.4 1.9±0.4 17±4.0	2.7±1.0 0.6±0.2 4.5±0.9
27 °C, 2 g/l	16.8±4.4 0.7±0.3 9.2±3.3	43.0±12.1 3.1±0.8 21.7±7.4	46.6±10.1 2.4±0.8 22.7±7.1	2.5±1.7 0.6±0.6 8.5±2.8
27 °C, 4 g/l	23.2±5.0 1.1±0.4 13.5±3.3	38.9±9.6 2.1±0.5 16.4±3.9	20.6±7.0 1.6±0.4 16.7±5.1	X X X
37 °C, 2 g/l	3.2±1.3 0.6±0.2 5.2±1.4	11.0±3.1 1.1±0.4 14.9±4.2	9.6±3.8 0.6±0.2 10.2±2.7	3.0±1.3 0.9±0.3 X
37 °C, 4 g/l	1.8±1.1 0.2±0.1 2.6±0.5	9.0±2.4 1.0±0.4 3.1±0.7	3.8±1.5 0.9±0.3 4.8±1.2	X X X

Condition Temperature, Solid Content	[Na$_2$SO$_4$]=5 mM Fiber Length Fiber Width Pore Size (μm)	[Na$_2$SO$_4$]=10 mM Fiber Length Fiber Width Pore Size (μm)	[Na$_2$SO$_4$]=20 mM Fiber Length Fiber Width Pore Size (μm)	[Na$_2$SO$_4$]=150mM Fiber Length Fiber Width Pore Size (μm)
RT, 2 g/l	36.2±12.3 5.3±1.9 64.9±16.7	50.2±11.3 6.4±2.1 36.7±11.8	49.3±16.0 3.5±1.2 39.2±14.2	52.8±23.9 1.2±0.22 49.9±14.5
RT, 4 g/l	39.3±15.3 5.1±1.4 43.4±11.6	37.1±9.6 4.8±1.1 53.1±16.3	47.5±11.6 3.3±0.7 47.1±11.5	71.9±17.9 1.5±0.3 35.1±8.8
37 °C, 2 g/l	22.0±8.2 1.6±0.3 16.6±4.4	24.6±5.9 1.7±0.3 14.1±2.9	24.2±6.0 1.54±0.2 8.8±2.8	25.6±5.7 1.56±0.3 19±3.7
37 °C, 4 g/l	13.8±5.9 1.1±0.3 7.8±2.4	19.1±6.1 1.3±0.4 16.5±4.7	22.5±5.2 1.4±0.2 11.8±4.1	19.2±4.6 1.6±0.2 22.8±5.9

1
2
3
4
5
6
7
8
9
10
11
12
13
14
15
16
17
18
19
20
21
22
23
24
25
26
27
28
29
30
31
32
33
34
35
36
37
38
39
40
41
42
43
44
45
46
47
48
49
50
51
52
53
54
55
56
57
58
59
60

24x7mm (300 x 300 DPI)